Observation of direct evolution from antiferromagnetism to superconductivity in $Cu_{1-x}Li_xFeAs$ $(0 \leqslant x \leqslant 1.0)$

Kunkun Li,[1,2] Duanduan Yuan,[1,2] Jiangang Guo,[1,*] and Xiaolong Chen[1,3,4,†]

[1]*Beijing National Laboratory for Condensed Matter Physics, Institute of Physics, Chinese Academy of Sciences, Beijing 100190, China*

[2]*University of Chinese Academy of Sciences, Beijing 100049, China*

[3]*School of Physical Sciences, University of Chinese Academy of Sciences, Beijing 101408, China*

[4]*Collaborative Innovation Center of Quantum Matter, Beijing 100084, China*

(Received 4 February 2018; revised manuscript received 19 March 2018; published 5 April 2018)

We report the structure, antiferromagnetism, and superconductivity in $Cu_{1-x}Li_xFeAs$ $(0 \leqslant x \leqslant 1.0)$ samples. A direct evolution from antiferromagnetism to superconductivity is observed as increasing doping level of Li. A phase diagram is constructed to show this evolution, which features no coexistence region between superconductivity and antiferromagnetism. This behavior shows that antiferromagnetic CuFeAs can be regarded as a parent compound to the observed superconductivity by equivalent doping, which is different from the cases with other FeAs-based superconductors. Structural analyses and first-principles calculations indicate that the anion height of Fe_2As_2 tetrahedral layer plays a crucial role on the physical properties. Moreover, the simple Fermi surface nesting picture adopted to explain the evolution from spin-density wave to superconductor in other FeAs-based superconductors might be not applicable to $Cu_{1-x}Li_xFeAs$.

DOI: 10.1103/PhysRevB.97.134503

I. INTRODUCTION

Since the discovery of iron-based superconductors in 2008, the interplay of unconventional superconductivity and magnetism has motivated extensive research to understand the pairing mechanism [1,2]. In copper oxide superconductors, the parent compounds are antiferromagnetic (AFM) Mott insulators with strong electron correlations and localized magnetic moments [3,4]. Superconductivity emerges after suppressing the static AFM order by doping carriers. Unlike copper oxides, the parent compounds of iron-based superconductors, such as LaOFeAs (1111) and $BaFe_2As_2$ (122), undergo an antiferromagnetic spin-density wave (SDW) transition, which is related to the peculiar Fermi surface (FS) nesting based on theoretical and experimental results [5–10]. In the momentum space, two kinds of nearly cylinder Fermi surfaces, hole pocket and electron pocket, at the Γ (0,0) point and M $(0,\pi)$ point, respectively, can be connected by nesting vectors [11,12]. These nesting vectors are usually equal to the antiferromagnetic wave vector as revealed by neutron-diffraction experiments [13–15]. Upon electron or hole doping, the static SDW order and FS nesting are gradually weakened and the superconductivity ensues [16].

LiFeAs has similar $FeAs_4$ tetrahedra as in other FeAs-based superconductors but shows superconductivity without any carrier doping [17,18]. It does not undergo the structural and AFM transitions. Low levels of doping (∼10 at. %) other 3*d* transition metals on Fe site in LiFeAs suppresses the superconductivity rapidly, while in other FeAs-based compounds, similar doping suppresses the SDW order and induces superconductivity [19–22]. The band-structure calculations of LiFeAs map out FSs with much shallower hole pockets around the Γ (0,0) point in comparison to that in 122 and 1111 superconductors [23–25]. The angle resolved photoemission spectroscopy study finds poor FS nesting and large renormalization of bands in the electronic structure [26]. Thus, the superconducting mechanism in FeAs-based family cannot simply be attributed to the FS nesting of itinerant electrons, and the strong electron correlations also play an important role [27].

Recently, the crystal structure and AFM state of CuFeAs were reported. It is isostructural to LiFeAs, consisting of alternate stacking Cu^+ layers and Fe_2As_2 layers [28]. The magnetic susceptibility measurements show that CuFeAs exhibits an AFM transition at $T_N \sim 9$ K or ferromagnetism (FM) transition at 42 K [28,29]. The neutron-diffraction and specific-heat measurements demonstrate that nonstoichiometric $Cu_xFe_{1-y}As$ exhibits collinear *G*-type AFM order at the Néel temperature $T_{N1} = 220$ K and canted AFM state at $T_{N2} = 140$ K [30]. First-principles calculations demonstrate that the anion height (h_{As}) is a key tuning parameter for the ground state, and it can switch the ground state from the AFM state to FM state [31,32]. The isostructual CuFeAs and LiFeAs offer an opportunity to investigate the correlation between superconductivity and magnetism in $Cu_{1-x}Li_xFeAs$. Here we report Li doping effect on structure and physical properties of $Cu_{1-x}Li_xFeAs$ samples with no disturbance of the Fe_2As_2 layer and no introduction of carriers. The study of this system allows us to establish a phase diagram showing how the antiferromagnetism of parent compound is suppressed and the superconductivity emerges by equivalent doping. Structural analyses, first-principles calculations, and physical property measurements illustrate that the h_{As} of Fe_2As_2 layer plays a crucial role in determining the physical properties in this solid solution.

*Corresponding author: jgguo@iphy.ac.cn

†Corresponding author: chenx29@iphy.ac.cn

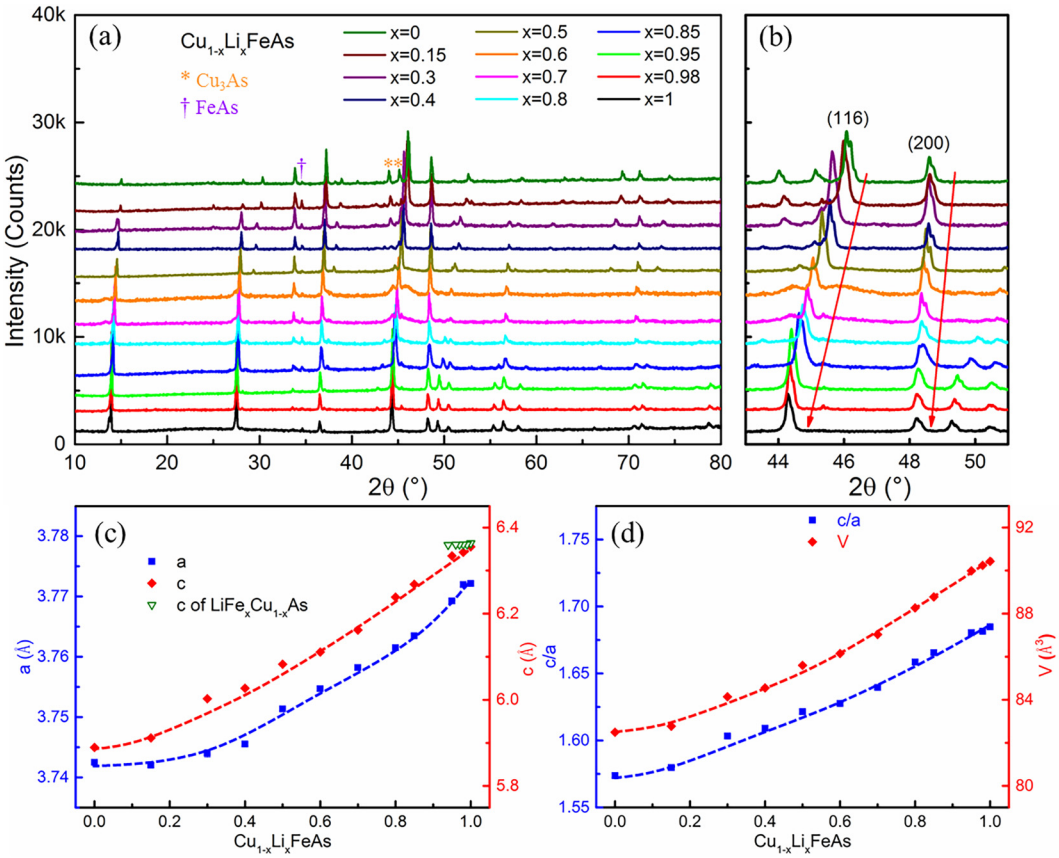

FIG. 1. (a) Powder x-ray diffraction patterns of $Cu_{1-x}Li_xFeAs$ samples. The impurity phases are marked by the symbols shown in parentheses, Cu_3As(*) and FeAs(†). (b) Enlarged (116) and (200) peaks. (c) Lattice parameters as a function of Li nominal content x for $Cu_{1-x}Li_xFeAs$. Inverted hollow triangles with green color represent the doping dependence of c in $LiFe_xCu_{1-x}As$ from Ref. [21]. (d) The c/a ratio and unit-cell volume with increasing Li content for $Cu_{1-x}Li_xFeAs$.

II. EXPERIMENTAL

Polycrystalline samples of $Cu_{1-x}Li_xFeAs$ were prepared via conventional solid-state method using alkali metal Li, Fe powder, Cu powder, and As powder (Alfa, 99.95, 99.999, 99.999, and 99.99%, respectively) as starting materials. FeAs precursors were prepared via the reaction of Fe and As powders at 1050 K for 24 h in sealed quartz tubes. The reground FeAs powder together with stoichiometric amount of Li and Cu was loaded into an alumina crucible, and then sealed into an evacuated quartz tube. The tube was subsequently annealed at 873 K for 24 h. After that, the obtained sample was pulverized, pressed into a pellet, sealed in a quartz tube with Ar gas, and then heated and kept at 973 K for 72 h. The obtained polycrystalline samples were dark gray and air-sensitive. Due to the sensitivity to air and moisture of raw materials, all operations were performed in an argon-filled glove box.

Room temperature powder x-ray diffraction (PXRD) data were collected using a PANalytical X'Pert PRO diffractometer (Cu Kα radiation) with a graphite monochromator in a reflection mode ($2\theta = 10$ to 130°, step $= 0.017^\circ$). Rietveld refinements were performed with the FULLPROF package [33]. The magnetic susceptibilities were measured using a vibrating sample magnetometer (Quantum Design). The electrical resistivity (ρ) measurements were carried out on a Physical Property Measurement System (Quantum Design) by a standard four-probe method.

First-principles calculations were performed using the CASTEP program code [34] with the plane-wave pseudopotential method, based on density-functional theory. We adopted the generalized gradient approximation with Perdew-Burke-Ernzerhof formula for the exchange-correlation potentials [35]. The ultrasoft pseudopotential with a plane-wave cutoff energy of 440 eV and a Monkhorst-Pack k-point separation of 0.02 $Å^{-1}$ in the reciprocal space were used for the calculations [36]. The self-consistent field was set as 5×10^{-7} eV/atom.

III. RESULTS AND DISCUSSION

Figure 1(a) displays the PXRD patterns of $Cu_{1-x}Li_xFeAs$ samples with $0 \leqslant x \leqslant 1.0$ collected at room temperature. The main phase can be well indexed by a tetragonal cell (space group $P4/nmm$). As for the undoped sample CuFeAs, the indexed pattern yields $a = 3.7425(3)$ Å, $c = 5.8897(7)$ Å, in good agreement with the previous reports [28]. Amounts of $Cu_3As(*)$ (~12 wt. %) and FeAs(†) (~5 wt. %) were observed as secondary phases, which were hard to be eliminated by various attempts. As shown in Fig. 1(b), (116) and (200) peaks of the main phase gradually shift to low diffraction angles with the increasing doping content of Li from 0 to 1. Both indexed

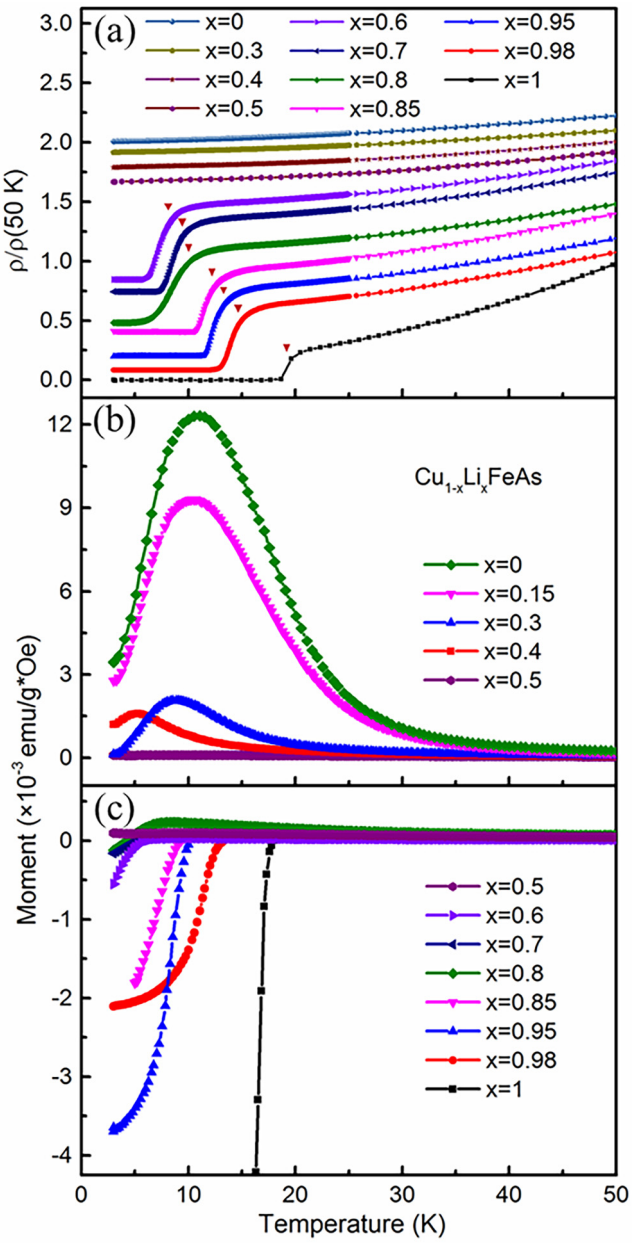

FIG. 2. (a) Electrical resistivity as a function of temperature for $Cu_{1-x}Li_xFeAs$ samples. For clarity, the data are normalized to $\rho(50\,K)$ and the resistivity curves have been offset. The superconducting transition temperatures are marked by red arrows. (b), (c) Temperature dependence of dc magnetic susceptibility under 40 Oe for $Cu_{1-x}Li_xFeAs$ samples ($x = 0 \sim 1.0$).

lattice parameters a and c expand monotonously, as plotted in Fig. 1(c), indicating no structural transition and a continuous solid solution in the whole doping range. For the end member of LiFeAs, the refined lattice parameters are $a = 3.7721(2)$ Å and $c = 6.3553(6)$ Å, respectively, consistent with previous reports [18]. As Li doping content x increases from 0 to 1, the a axis slightly lengthens by about 0.8% while the c axis expands by about 7.9%. Since the ionic size of Cu^+ ion (0.6 Å) is comparable to Li^+ ion (0.59 Å), such a large expansion of c axis is unsual. It is speculated that the increase of c as x increases is due to smaller electronegativity of Li (0.98) than Cu (1.90). The Li doping dependence of lattice parameter c in $Cu_{1-x}Li_xFeAs$ shows a distinct trend from that in $LiFe_xCu_{1-x}As$ [21], as shown in Fig. 1(c), indicating that Cu occupies the Li site in our samples rather than the Fe site as in $LiFe_xCu_{1-x}As$. Figure 1(d) shows the monotonic increase of the c/a ratio as well as the unit-cell volume of $Cu_{1-x}Li_xFeAs$ with increasing Li doping content. The increasing c/a ratio from 1.57 for CuFeAs to 1.68 for LiFeAs indicates that LiFeAs has a more two-dimensional structure than CuFeAs.

Figure 2(a) shows the temperature-dependent resistivity of $Cu_{1-x}Li_xFeAs$. For clarity, all of the resistivity data are normalized to $\rho(50\,K)$. For $0 \leqslant x \leqslant 0.5$, the resistivity data exhibit metallic behavior in the whole measured temperature region. As x reaches 0.6, a drastic drop of resistivity to zero starts to emerge, indicating a transition to the superconducting state. The superconducting transition temperature (T_c^{onset}), defined as the temperature at which resistivity drops by 10% of normal state resistivity, is ~9.2 K. The resistivity reaches zero (T_c^{zero}) at ~6.1 K. With further increasing the doping level of Li, T_c^{onset} is monotonically enhanced to ~19.3 K and T_c^{zero} increases to ~18.5 K for LiFeAs, consistent with that reported in LiFeAs ($T_c \sim 18\,K$) [17]. The temperature-dependent magnetic susceptibility under 40 Oe in zero-field cooling mode is shown in Figs. 2(b) and 2(c). It is found that parent CuFeAs shows an AFM transition with $T_N = 11.1\,K$, which is comparable to previous reports ($T_N \sim 9\,K$). But, no anomaly can be seen from resistivity data, indicating the observed AFM transition is not induced by FS nesting as usually observed in 122 and 1111 systems. The temperature-dependent susceptibility from 50 to 100 K can be fitted by the Curie-Weiss law $\chi = C/(T-\theta_{cw})$, where C is the Curie constant and θ_{cw} is the Weiss temperature. An effective moment of 1.82 μ_B can be obtained from the fitted Curie constant. T_N is suppressed gradually to 5.3 K at $x = 0.4$ and cannot be observed above 2 K at $x = 0.5$, where the effective moment decreases to 1.55 μ_B. Consistent with the resistivity data, the samples for $0.6 \leqslant x \leqslant 1$ display superconductivity as evidenced by a large Meissner effect at T_c. The susceptibility for $x = 0.6$ shows a superconducting transition at ~6.5 K. With further increasing the doping level of Li, T_c is enhanced to ~18.2 K for LiFeAs, slightly lower than T_c^{onset} from the resistivity data. The superconducting volume fraction of $Cu_{1-x}Li_xFeAs$ increases from an estimated value of 5% for $x = 0.6$ to 83% for $x = 1$.

The properties in FeAs-based superconductors are known to be strongly correlated to the geometry of $FeAs_4$ tetrahedron, and the optimal superconductor (SC) usually corresponds to a regular tetrahedron and an optimal anion height $h_{As} \sim 1.38$ Å, as illustrated in previous reports [37–39]. Thus, we carried out the Rietveld refinements for all the x-ray diffraction patterns and extracted the structural parameters of $FeAs_4$ tetrahedron. Figure 3(a) shows the geometry configuration of the Fe_2As_2 layer of $Cu_{1-x}Li_xFeAs$, which is made up of edge-sharing $FeAs_4$ tetrahedra with a square lattice of Fe atoms. Replacing Cu by Li brings out variation in Fe–As bond lengths, As–Fe–As angle, and h_{As}. As shown in Fig. 3(b), the Fe–As bond length decreases from 2.442(3) to 2.402(1) Å. Meanwhile, the As–Fe–As angle α increases from 100.0(1) to 103.5(1)° while the

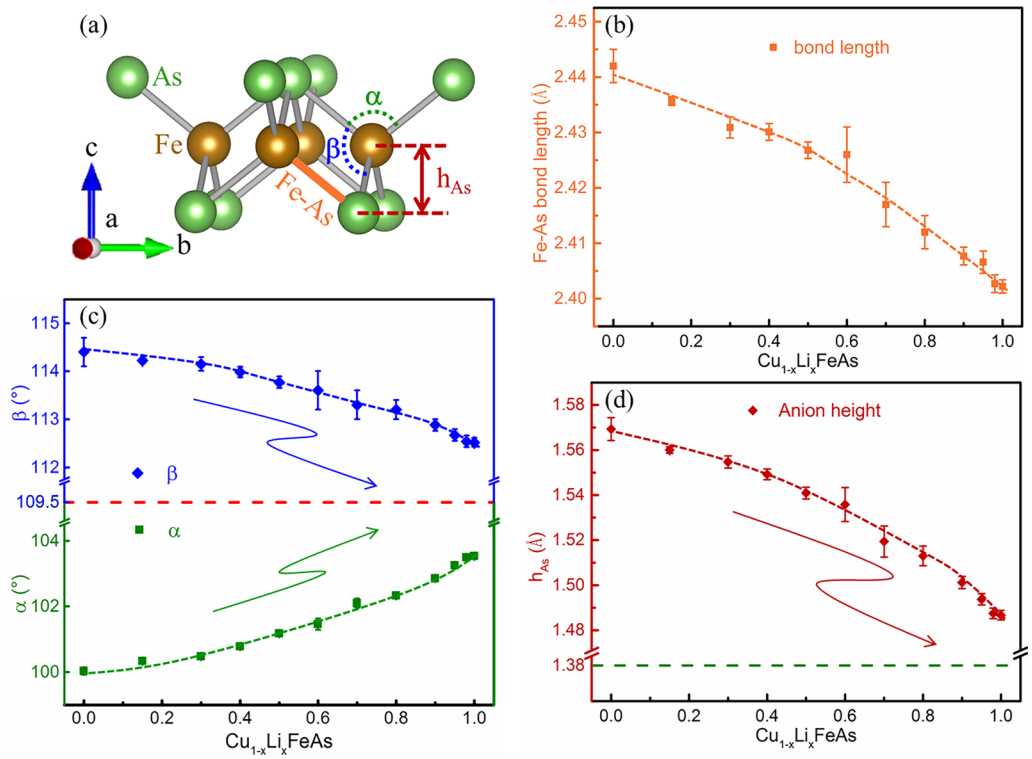

FIG. 3. (a) Fe_2As_2 layer extracted from the crystal structure. (b) Fe–As bond length dependence as a function of Li content x for $Cu_{1-x}Li_xFeAs$ ($x = 0 \sim 1.0$). (c) As–Fe–As bond angle dependence as a function of Li content x. The red dashed line represents the regular $FeAs_4$ tetrahedron angle of 109.5°. (d) Anion height dependence as a function of Li content x. The green dashed line represents the optimal $h_{As} = 1.38$ Å with the highest T_c reported in FeAs-based superconductors.

As–Fe–As bond angle β decreases from 114.4(3) to 112.5(1)°, as shown in Fig. 3(c). Since a regular tetrahedron has an ideal angle of 109.5°, we can infer the $FeAs_4$ tetrahedron approaches the regular one as Li content increases, which might be responsible for the emergence of superconductivity. The h_{As}, which is a comprehensive parameter reflecting variations in both Fe–As bond lengths and the As–Fe–As angles, decreases from 1.570(5) to 1.487(2) Å, approaching to the optimal h_{As} of 1.38 Å, as shown in Fig. 3(d). As in previous reports, theoretical calculations suggest that the Fe–As bond length directly affects the coupling interaction between the Fe and As atoms, and Fe electrons become more itinerant with decreasing Fe–As bond length [40]. The tetrahedron shape, which is parametrized in terms of the As–Fe–As bond angles, affects the crystal-field levels and the orbital occupancies. It is reported that superconductors with regular $FeAs_4$ tetrahedron possess the optimal T_c. On the other hand, the h_{As} is correlated to the direct hopping between the nearest Fe-Fe and indirect Fe-Fe hopping through the As atoms. Through tuning the h_{As}, the ground state of FeAs-based compounds can be altered [32,40]. In $BaFe_2(As_{1-x}P_x)_2$ and $SrFe_2As_{2-y}P_y$, the anion height linearly decreases as equivalent P-doping level increases. As a result, the SDW is suppressed and dome-shaped superconductivity is observed [41,42]. In $Cu_{1-x}Li_xFeAs$, the refined h_{As} decreases from 1.570(5) to 1.487(2) Å with increasing Li. Similarly, the AFM ground state is suppressed and superconductivity ensues. In addition, we note that a moderate value of h_{As} (1.570 Å) renders CuFeAs in an AFM ground state; a higher value of h_{As} (1.84 Å) can drive this system toward an FM order, as evidenced by the fact that CuFeAs is antiferromagnetic while CuFeSb is ferromagnetic [43].

We calculate the electronic structures of CuFeAs, $Li_{0.5}Cu_{0.5}FeAs$, and LiFeAs, and the results are shown in Figs. 4(a)–4(c), respectively. In the Γ-Z direction, the dispersion is weak for LiFeAs compared with $Li_{0.5}Cu_{0.5}FeAs$ and CuFeAs. This could be expected considering the elongated c axis as well as the large c/a ratio by doping of Li. Thus, it can be inferred that $Cu_{1-x}Li_xFeAs$ exhibits a more two-dimensional character in electronic structure as x increases. The band structure around the Fermi level shows similar electron and hole pocket geometry for CuFeAs and $Li_{0.5}Cu_{0.5}FeAs$. However, there are some distinctions for LiFeAs. As can be seen, there are two electron pockets around the M and A points and one hole pocket around the Γ point for CuFeAs and $Li_{0.5}Cu_{0.5}FeAs$. In the case of LiFeAs, there are two electron pockets around the M and A points and three hole pockets around the Γ point, which is consistent with previous reports [25,44]. As the doping level x increases, two shallow hole pockets around the Γ point gradually emerge, which can provide a better nesting environment compared with CuFeAs and $Li_{0.5}Cu_{0.5}FeAs$. This indispensable FS nesting is an essential condition to the spin-fluctuation-mediated superconductivity [23]. We also noticed that according to our calculations, the band width across the Fermi surface decreases slightly as Li doping level increases.

The total and partial densities of states (DOS) of CuFeAs, $Li_{0.5}Cu_{0.5}FeAs$, and LiFeAs are shown in Figs. 4 (d)–4(f). The states near the Fermi energy mainly consist of the Fe 3d electrons, slightly hybridized with As 4p electrons. The Cu 3d

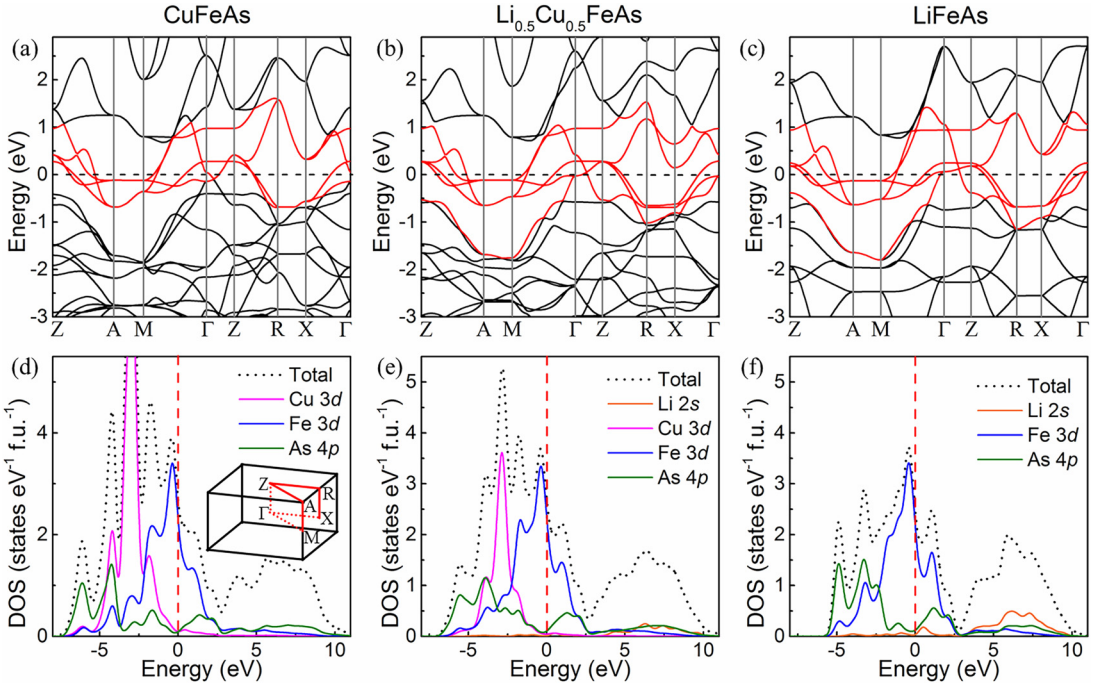

FIG. 4. (a)–(c) Calculated band structures of CuFeAs, $Li_{0.5}Cu_{0.5}FeAs$, and LiFeAs, respectively. (d)–(f) Total and partial DOS of CuFeAs, $Li_{0.5}Cu_{0.5}FeAs$, and LiFeAs, respectively. The inset in (d) is the first Brillouin zone.

electrons mainly contribute to the states near −2.9 eV, with few 3*d* states contributing to the Fermi surface. Therefore, the Cu 3*d* orbitals are nearly fully occupied in these compounds with $3d^{10}$ electronic configuration and Cu atoms have a formal valence state of Cu^{+}, suggesting that Li substitution for Cu in $Cu_{1-x}Li_xFeAs$ should be an equivalent doping effect [45]. The calculated total DOS for CuFeAs, $Li_{0.5}Cu_{0.5}FeAs$, and LiFeAs are 2.7 states eV^{-1} Fe^{-1}, 2.65 states eV^{-1} Fe^{-1}. and 2.5 states eV^{-1} Fe^{-1}, respectively. The slight change of DOS should originate from the difference in $FeAs_4$ tetrahedra of CuFeAs, $Li_{0.5}Cu_{0.5}FeAs$, and LiFeAs, which cannot explain the evolution from AFM to SC, implying the emergence of SC should relate to the other mechanism like the strong magnetic fluctuation [46].

The phase diagram of $Cu_{1-x}Li_xFeAs$ is shown in Fig. 5, including AFM and SC transition temperatures as a function of Li doping content. As can be seen, the AFM is suppressed with increasing Li content. When the AFM totally vanishes at $x = 0.5$, the SC immediately starts to emerge, exhibiting two distinct regions. A similar phenomenon has been observed in $CeFeAsO_{1-x}F_x$ [47]; thus, CuFeAs could be regarded as a parent compound to the observed superconductivity. This phase diagram is quite different from those in the 1111 and 122 systems. For the 122 parent compound, there is a tetragonal to orthogonal structure transition followed by a SDW transition. Through doping, the SDW order and FS nesting are gradually weakened and the superconductivity ensues. A microscopically coexistence region of SC and short-range AFM order in light-doped samples is usually observed [48,49]. With further doping, the SDW order is totally suppressed and superconductivity occurs. In the case of LiFeAs, the strong size mismatch between the electron pockets at the *M* point and the relatively small hole pockets at the Γ point indicates that the FS nesting effect is weak, and superconductivity emerges without any carrier doping. But, unlike the SDW induced by FS nesting in 122 parent compounds, the observed AFM in CuFeAs is not the case, as evidenced by the absence of anomaly in resistivity data and first-principles calculations results that the two small hole pockets at the Γ point sink below the Fermi level. Thus, the FS nesting picture used to explain the evolution from SDW to SC in 122 systems might be inappropriate in $Cu_{1-x}Li_xFeAs$. As reported in $BaFe_2(As_{1-x}P_x)_2$ and $SrFe_2As_{2-y}P_y$, while the anion height decreases linearly without any carrier doping, the

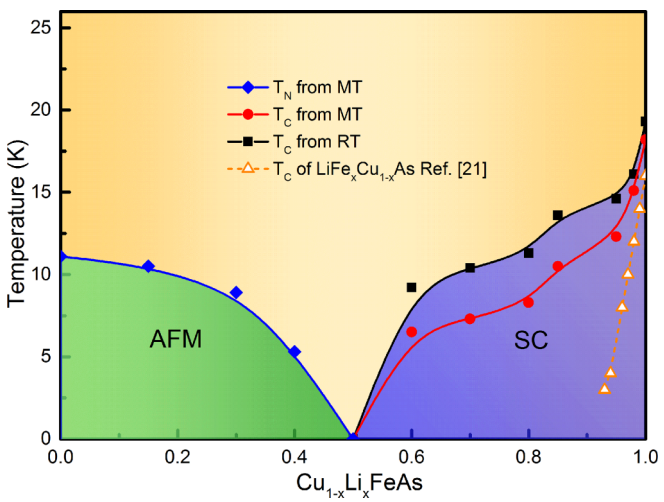

FIG. 5. Doping dependence of electronic phase diagram of $Cu_{1-x}Li_xFeAs$. The blue and red symbols represent T_N and T_c extracted from susceptibility data. The black squares represent T_c extracted from resistivity data. The yellow hollow triangles represent the doping dependence of T_c in $LiFe_xCu_{1-x}As$ from Ref. [21].

SDW state is suppressed and the dome-shaped superconducting phase appears [41,42]. Similarly, in our case, the decreases of h_{As} from 1.570(5) to 1.487(2) Å in $Cu_{1-x}Li_xFeAs$ plays an important role when tuning the ground state from AFM to superconductivity.

In comparison, the SC transition temperatures of $LiFe_xCu_{1-x}As$ are also presented in Fig. 5, and the superconductivity of $LiFe_xCu_{1-x}As$ is quickly quenched at $x > 0.9$ [21]. In the isostructural $NaFe_xCu_{1-x}As$, SDW is suppressed and a dome-shaped superconductivity emerges with the complete suppression of superconductivity at $x = 0.95$ [50]. Further increasing the doping level would result in a Mott insulator at $x = 0.5$, because of strong electronic correlations induced by Cu^+ [51]. Comparing with $NaFe_xCo_{1-x}As(T_c^{max} = 20\,K)$, the relatively low optimal T_c of 11.8 K suggests that the impurity potential of Cu is stronger than that of Co in NaFeAs [52]. In $Cu_{1-x}Li_xFeAs$, superconductivity persists up to $Cu_{0.4}Li_{0.6}FeAs$. Thus, this equivalent substitution with no disturbance on Fe_2As_2 layer offers an opportunity to investigate the influence of $FeAs_4$ tetrahedron geometry on superconductivity in FeAs-based 111 systems.

In conclusion, we report studies on Li doping at Cu site in $Cu_{1-x}Li_xFeAs$ compounds. A continuous solid solution from CuFeAs to LiFeAs is achieved. The effects of equivalent doping on the evolution of structure, antiferromagnetism, and superconductivity are studied. We found that anion height h_{As} is crucial when tuning the antiferromagnetism and superconductivity among $Cu_{1-x}Li_xFeAs$ compounds. Different from the reported coexistence and competition of antiferromagnetic order and superconductivity in 1111 and 122 systems, no coexistence of antiferromagnetic order and superconductivity can be observed in $Cu_{1-x}Li_xFeAs$. These results provide more experimental clues to understand the inherent superconducting mechanism in FeAs-based superconductors.

ACKNOWLEDGMENTS

This work is financially supported by the National Natural Science Foundation of China (Grants No. 51532010, No. 91422303, and No. 51772322), the National Key Research and Development Program of China (Grants No. 2016YFA0300600 and No. 2017YFA0304700), Beijing Municipal Science & Technology Commission (Grant No. Z161100002116018), the Strategic Priority Research Program of the Chinese Academy of Sciences (Grant No. XDB07020100), and the Chinese Academy of Sciences (Grant No. QYZDJ-SSWSLH013).

[1] Y. Kamihara, T. Watanabe, M. Hirano, and H. Hosono, J. Am. Chem. Soc. **130**, 3296 (2008).
[2] M. Rotter, M. Tegel, and D. Johrendt, Phys. Rev. Lett. **101**, 107006 (2008).
[3] J. G. Bednorz and K. A. Müller, Z. Phys. B **64**, 189 (1986).
[4] N. Yoshikazu, T. Madoka, M. Keizo, and U. Hiromi, Jpn. J. Appl. Phys. **26**, L1416 (1987).
[5] M. Rotter, M. Tegel, D. Johrendt, I. Schellenberg, W. Hermes, and R. Pöttgen, Phys. Rev. B **78**, 020503 (2008).
[6] D. J. Singh and M. H. Du, Phys. Rev. Lett. **100**, 237003 (2008).
[7] D. J. Singh, Phys. Rev. B **78**, 094511 (2008).
[8] I. I. Mazin, D. J. Singh, M. D. Johannes, and M. H. Du, Phys. Rev. Lett. **101**, 057003 (2008).
[9] K. Kuroki, H. Usui, S. Onari, R. Arita, and H. Aoki, Phys. Rev. B **79**, 224511 (2009).
[10] F. Wang, H. Zhai, Y. Ran, A. Vishwanath, and D.-H. Lee, Phys. Rev. Lett. **102**, 047005 (2009).
[11] M. Yi, D. H. Lu, J. G. Analytis, J. H. Chu, S. K. Mo, R. H. He, R. G. Moore, X. J. Zhou, G. F. Chen, J. L. Luo, N. L. Wang, Z. Hussain, D. J. Singh, I. R. Fisher, and Z. X. Shen, Phys. Rev. B **80**, 024515 (2009).
[12] F. Ma, Z.-Y. Lu, and T. Xiang, Phys. Rev. B **78**, 224517 (2008).
[13] C. R. DelaCruz, Q. Huang, J. W. Lynn, J. Y. Li, W. R. Ii, J. L. Zarestky, H. A. Mook, G. F. Chen, J. L. Luo, N. L. Wang, and P. Dai, Nature (London) **453**, 899 (2008).
[14] Q. Huang, Y. Qiu, W. Bao, M. A. Green, J. W. Lynn, Y. C. Gasparovic, T. Wu, G. Wu, and X. H. Chen, Phys. Rev. Lett. **101**, 257003 (2008).
[15] K. Kuroki, S. Onari, R. Arita, H. Usui, Y. Tanaka, H. Kontani, and H. Aoki, Phys. Rev. Lett. **101**, 087004 (2008).
[16] J. P. Castellan, S. Rosenkranz, E. A. Goremychkin, D. Y. Chung, I. S. Todorov, M. G. Kanatzidis, I. Eremin, J. Knolle, A. V. Chubukov, S. Maiti, M. R. Norman, F. Weber, H. Claus, T. Guidi, R. I. Bewley, and R. Osborn, Phys. Rev. Lett. **107**, 177003 (2011).
[17] X. C. Wang, Q. Q. Liu, Y. X. Lv, W. B. Gao, L. X. Yang, R. C. Yu, F. Y. Li, and C. Q. Jin, Solid State Commun. **148**, 538 (2008).
[18] M. J. Pitcher, D. R. Parker, P. Adamson, S. J. C. Herkelrath, A. T. Boothroyd, R. M. Ibberson, M. Brunelli, and S. J. Clarke, Chem. Commun. **0**, 5918 (2008).
[19] L. Y. Xing, X. Shi, P. Richard, X. C. Wang, Q. Q. Liu, B. Q. Lv, J. Z. Ma, B. B. Fu, L. Y. Kong, H. Miao, T. Qian, T. K. Kim, M. Hoesch, H. Ding, and C. Q. Jin, Phys. Rev. B **94**, 094524 (2016).
[20] S. Aswartham, G. Behr, L. Harnagea, D. Bombor, A. Bachmann, I. V. Morozov, V. B. Zabolotnyy, A. A. Kordyuk, T. K. Kim, D. V. Evtushinsky, S. V. Borisenko, A. U. B. Wolter, C. Hess, S. Wurmehl, and B. Buchner, Phys. Rev. B **84**, 054534 (2011).
[21] L. Y. Xing, H. Miao, X. C. Wang, J. Ma, Q. Q. Liu, Z. Deng, H. Ding, and C. Q. Jin, J. Phys.: Condens. Matter **26**, 435703 (2014).
[22] L. Y. Xing, X. C. Wang, Z. Deng, Q. Q. Liu, and C. Q. Jin, Phys. C Supercond. **493**, 141 (2013).
[23] G. Lee, H. S. Ji, Y. Kim, C. Kim, K. Haule, G. Kotliar, B. Lee, S. Khim, K. H. Kim, K. S. Kim, K. S. Kim, and J. H. Shim, Phys. Rev. Lett. **109**, 177001 (2012).
[24] A. Lankau, K. Koepernik, S. Borisenko, V. Zabolotnyy, B. Büchner, J. van den Brink, and H. Eschrig, Phys. Rev. B **82**, 184518 (2010).
[25] I. A. Nekrasov, Z. V. Pchelkina, and M. V. Sadovskii, JETP Lett. **88**, 543 (2008).

[26] S. V. Borisenko, V. B. Zabolotnyy, D. V. Evtushinsky, T. K. Kim, I. V. Morozov, A. N. Yaresko, A. A. Kordyuk, G. Behr, A. Vasiliev, R. Follath, and B. Buchner, Phys. Rev. Lett. **105**, 067002 (2010).
[27] M. D. Johannes and I. I. Mazin, Phys. Rev. B **79**, 220510 (2009).
[28] G. S. Thakur, Z. Haque, L. C. Gupta, and A. K. Ganguli, J. Phys. Soc. Jpn. **83**, 054706 (2014).
[29] B. Qian, J. Hu, J. Liu, Z. Han, P. Zhang, L. Guo, X. Jiang, T. Zou, M. Zhu, C. R. DelaCruz, X. Ke, and Z. Q. Mao, Phys. Rev. B **91**, 014504 (2015).
[30] T. Zou, C. C. Lee, W. Tian, H. B. Cao, M. Zhu, B. Qian, C. R. dela Cruz, W. Ku, Z. Q. Mao, and X. Ke, Phys. Rev. B **95**, 054414 (2017).
[31] G. Wang, X. Shi, and D. Wang, J. Alloys Compd. **686**, 38 (2016).
[32] W. G. Yin, C. C. Lee, and W. Ku, Phys. Rev. Lett. **105**, 107004 (2010).
[33] J. Rodríguez-Carvajal, Physica B: Condens. Matter **192**, 55 (1993).
[34] S. J. Clark, M. D. Segall, C. J. Pickard, P. J. Hasnip, M. I. J. Probert, K. Refson, and M. C. Payne, Z. Kristallogr. **220**, 567 (2005).
[35] J. P. Perdew, K. Burke, and M. Ernzerhof, Phys. Rev. Lett. **77**, 3865 (1996).
[36] H. J. Monkhorst and J. D. Pack, Phys. Rev. B **13**, 5188 (1976).
[37] Y. Mizuguchi, Y. Hara, K. Deguchi, S. Tsuda, T. Yamaguchi, H. Kotegawa, H. Tou, and Y. Takano, Supercond. Sci. Technol. **23**, 054013 (2010).
[38] C. H. Lee, K. Kihou, A. Iyo, H. Kito, P. M. Shirage, and H. Eisaki, Solid State Commun. **152**, 644 (2012).
[39] X. Chen, N. Liu, J. Guo, and X. Chen, Phys. Rev. B **96**, 134519 (2017).
[40] Z. P. Yin, K. Haule, and G. Kotliar, Nat. Mater. **10**, 932 (2011).
[41] T. Kobayashi, S. Miyasaka, S. Tajima, and N. Chikumoto, J. Phys. Soc. Jpn. **83**, 104702 (2014).
[42] S. Kasahara, T. Shibauchi, K. Hashimoto, K. Ikada, S. Tonegawa, R. Okazaki, H. Shishido, H. Ikeda, H. Takeya, K. Hirata, T. Terashima, and Y. Matsuda, Phys. Rev. B **81**, 184519 (2010).
[43] B. Qian, J. Lee, J. Hu, G. C. Wang, P. Kumar, M. H. Fang, T. J. Liu, D. Fobes, H. Pham, L. Spinu, X. S. Wu, M. Green, S. H. Lee, and Z. Q. Mao, Phys. Rev. B **85**, 144427 (2012).
[44] Z. J. Chen, G. B. Xu, J. G. Yan, Z. Kuang, T. H. Chen, and D. H. Li, J. Appl. Phys. **120**, 235103 (2016).
[45] D. J. Singh, Phys. Rev. B **79**, 153102 (2009).
[46] I. Tetsuya, N. Yusuke, K. Shunsaku, I. Kenji, I. Hiroaki, K. Shigeru, S. Takasada, M. Yuji, and T. Takahito, J. Phys.: Conf. Ser. **391**, 012127 (2012).
[47] J. Zhao, Q. Huang, C. R. DelaCruz, S. Li, J. W. Lynn, Y. Chen, M. A. Green, G. F. Chen, G. Li, Z. Li, J. L. Luo, N. L. Wang, and P. Dai, Nat. Mater. **7**, 953 (2008).
[48] H. Luo, R. Zhang, M. Laver, Z. Yamani, M. Wang, X. Lu, M. Wang, Y. Chen, S. Li, S. Chang, J. W. Lynn, and P. Dai, Phys. Rev. Lett. **108**, 247002 (2012).
[49] E. Wiesenmayer, H. Luetkens, G. Pascua, R. Khasanov, A. Amato, H. Potts, B. Banusch, H.-H. Klauss, and D. Johrendt, Phys. Rev. Lett. **107**, 237001 (2011).
[50] G. Tan, Y. Song, R. Zhang, L. Lin, Z. Xu, L. Tian, S. Chi, M. K. Graves-Brook, S. Li, and P. Dai, Phys. Rev. B **95**, 054501 (2017).
[51] Y. Song, Z. Yamani, C. Cao, Y. Li, C. Zhang, J. S. Chen, Q. Huang, H. Wu, J. Tao, Y. Zhu, W. Tian, S. Chi, H. Cao, Y. Huang, M. Dantz, T. Schmitt, R. Yu, A. H. Nevidomskyy, E. Morosan, Q. Si, and P. Dai, Nat. Commun. **7**, 13879 (2016).
[52] A. F. Wang, X. G. Luo, Y. J. Yan, J. J. Ying, Z. J. Xiang, G. J. Ye, P. Cheng, Z. Y. Li, W. J. Hu, and X. H. Chen, Phys. Rev. B **85**, 224521 (2012).